Comparison of H_2 Photogeneration by [FeFe]-Hydrogenase Mimics with CdSe QDs and $Ru(bpy)_3Cl_2$ in Aqueous Solution

Jing-Xin Jian†, Chen Ye†, Xu-Zhe Wang, Min Wen, Zhi-Jun Li, Xu-Bing Li, Bin Chen, Chen-Ho Tung and Li-Zhu Wu*

Key Laboratory of Photochemical Conversion and Optoelectronic Materials, Technical Institute of Physics and Chemistry & Graduate University, the Chinese Academy of Sciences, Beijing 100190, P. R. China. E-mail: lzwu@mail.ipc.ac.cn.

Table of Contents

1. Instruments and materials

Materials All chemicals were obtained from commercial suppliers and used without further purification unless otherwise noted.

Instruments Infrared spectra were recorded on a Nicolet NEXUS 670 FT-IR spectrophotometer. The UV-vis absorption spectra were recorded using a Shimadzu 1601 PC spectrophotometer. ^{1}H-NMR spectra were run on a Bruker-400 spectrometer with tetramethylsilane (1H) as an internal standard. MS was performed on a Bruker APEX III 7.0 Tesla FTICR Mass spectrometer combined with Apollo ESI source. Elemental analyses were determined on a FLASH EA1112 elemental analyzer. Electrochemical investigation was studied on a Princeton Applied Research Potentionstat-gravanostat model 283. Cyclic voltammetry experiments were obtained using a standard three electrode cell under argon at room temperature with a glassy carbon working electrode and a platinum wire auxiliary electrode. For aqueous system, saturated calomel electrode (SCE) was used as the reference electrode, and the supporting electrolyte solution was 0.1 M NaCl. All redox potentials are reported relative to the SCE and then adjusted to normal hydrogen electrode (NHE). Between each scan the glassy carbon electrode was removed and polished using a 0.05 μm polycrystalline diamond suspension and rinsed with both acetone and deionized water to remove any adsorbed material. All samples were run at a concentration of 1.0 mM.

2. ESI-MS spectrum of 1 and 2.

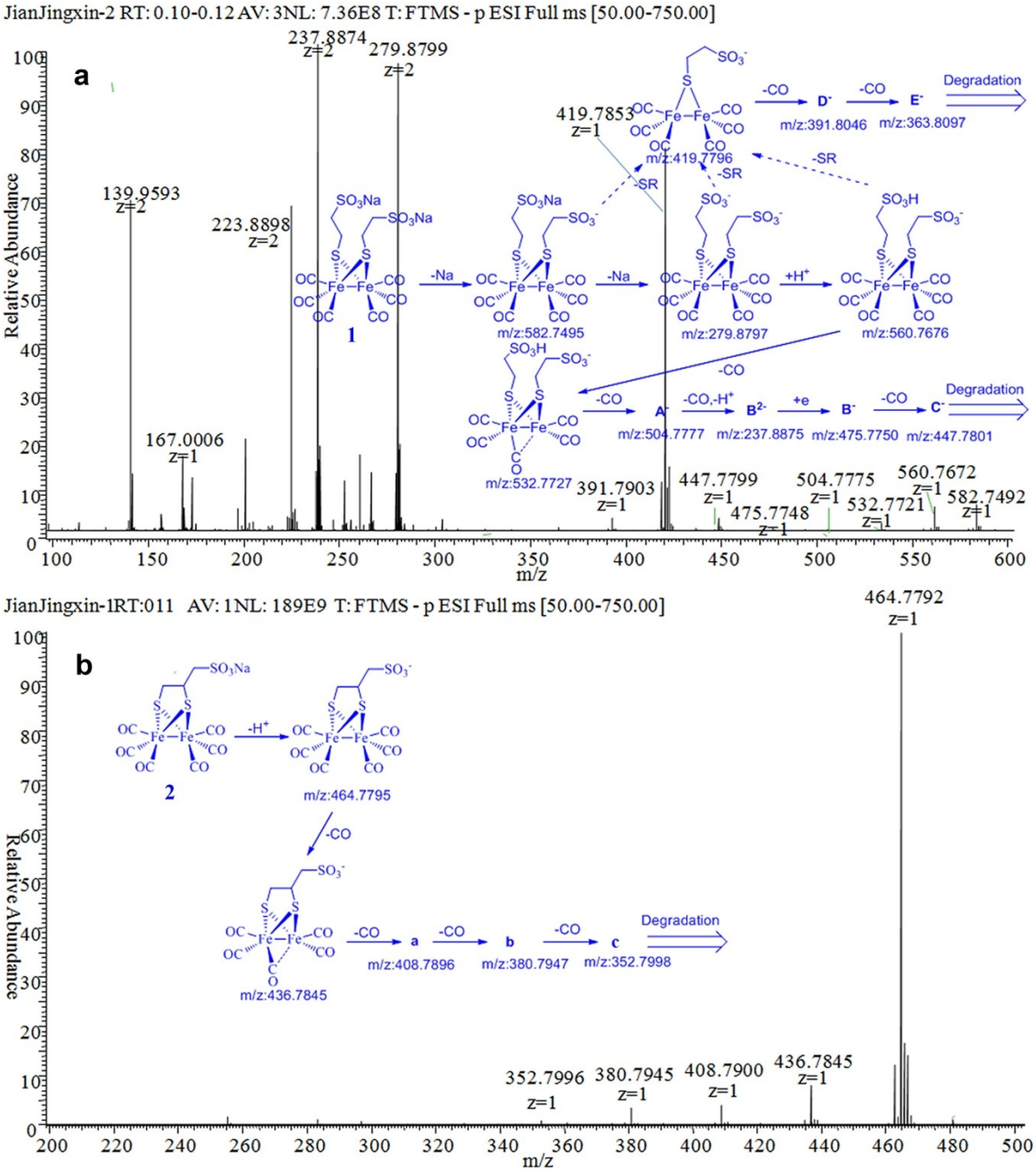

Fig. S1 ESI-MS spectrum of **1** (**a**) and **2** (**b**) in aqueous solution, and the supposed dissociation particles.

3. Absorption and emission of different size CdSe QDs

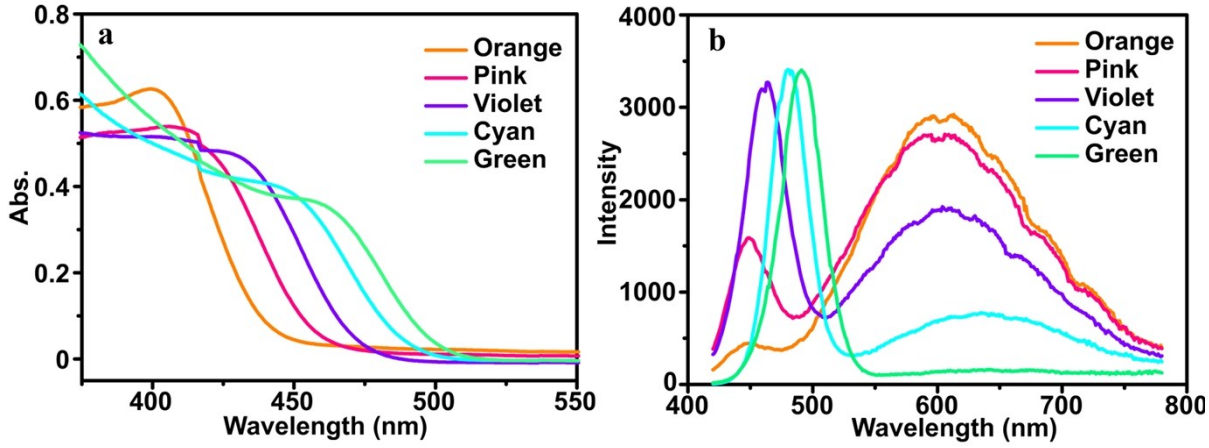

Fig. S2 The absorption spectra (**a**) and photoluminescence spectra (**b**) of different size CdSe QDs, the primary concentration of Cd^{2+} was 1.0 mM.

4. The optimization of H_2 photogeneration conditions.

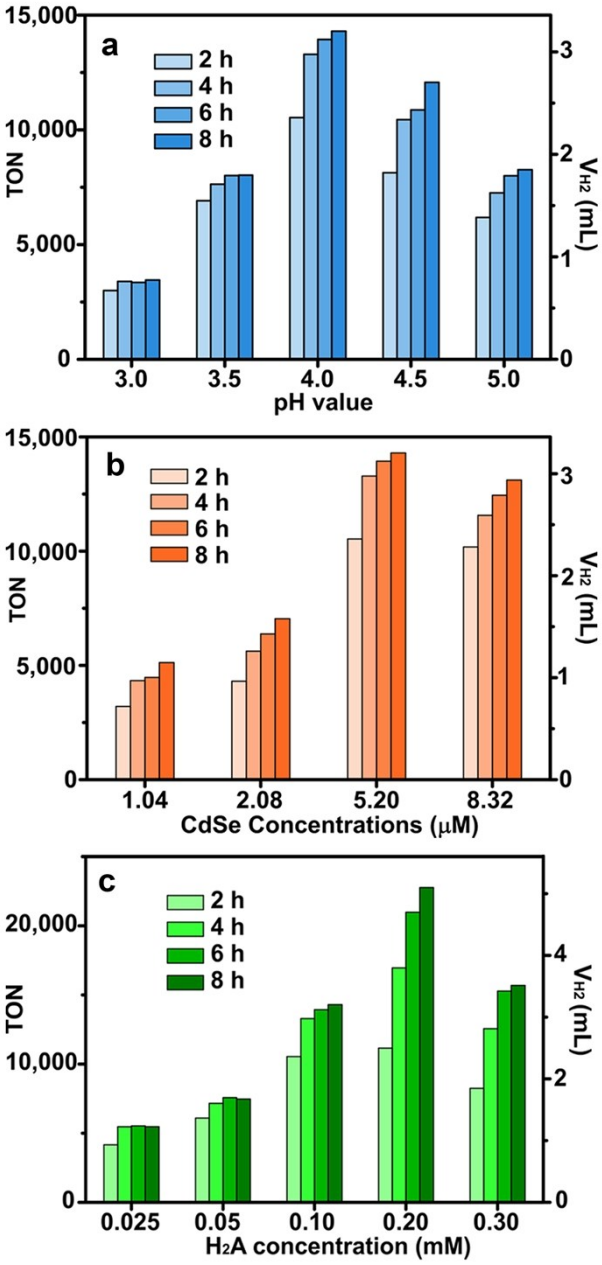

Fig. S3 Photocatalytic H_2 evolution at various pH values with **1** (1.00 μM), CdSe QDs (2.08 μM) and H_2A (0.10 M) in aqueous solution (**a**); H_2 evolution as function of CdSe concentration with **1** (1.00 μM) and H_2A (0.10 M) at pH 4.0 (**b**); H_2 evolution as function of H_2A concentration with **1** (1.00 μM) and CdSe (5.20 μM) at pH 4.0 (**c**).

5. The absorption characteristic and water solubility of 1.

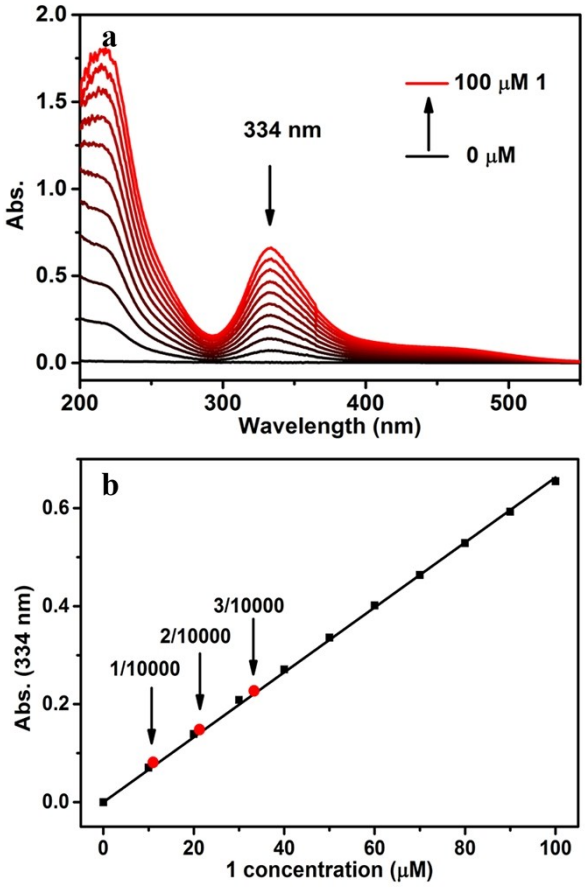

Fig. S4 The UV-vis absorption spectra of **1** in aqueous solution (**a**) and the standard solubility curve of **1** recorded at 334 nm (**b**).

6. HRTEM of CdSe QDs.

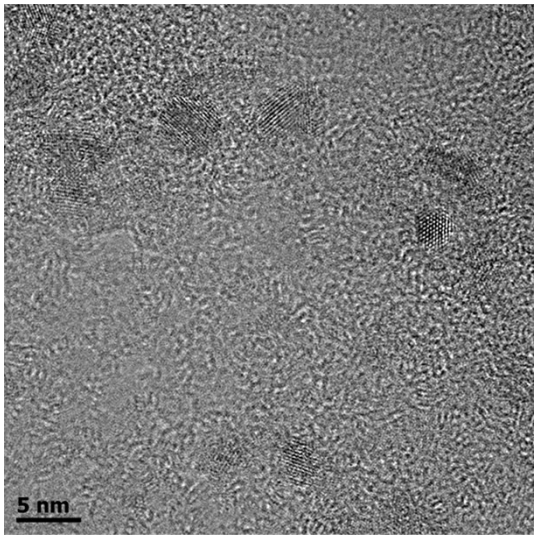

Fig. S5 High-resolution transmission electron microscopy image of MPA-CdSe QDs (bar scale, 5 nm).

7. H_2 evolution without [FeFe]-H_2ase mimics.

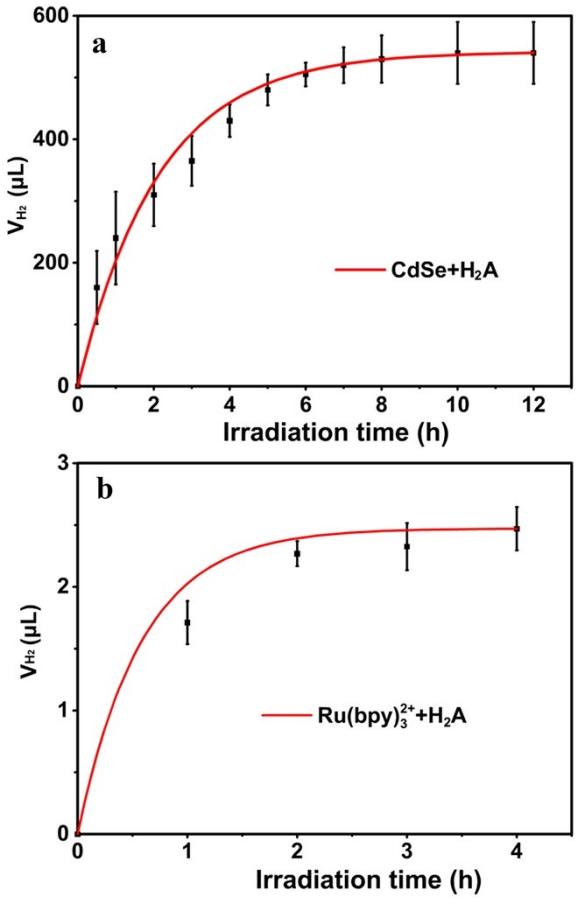

Fig. S6 Photocatalytic H_2 evolution of $Ru(bpy)_3^{2+}$ (0.10 mM) and H_2A (0.20 M) at pH 4.0 (**a**); photocatalytic H_2 evolution of CdSe QDs (2.08 μM) and H_2A (0.20 M) at pH 4.0 (**b**).

8. Cyclic voltammetry of 1 and 2.

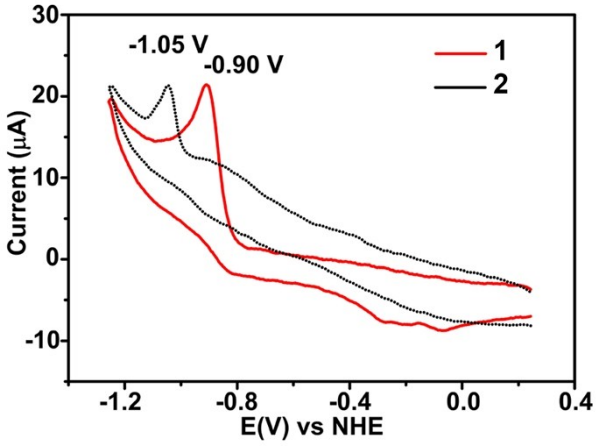

Fig. S7 Cyclic voltammetry of **1** (1.0 mM) and **2** (1.0 mM) in aqueous solution at scan rate of 50 mV/s.

9. Emission quenching of $Ru(bpy)_3Cl_2$ by 1 and 2.

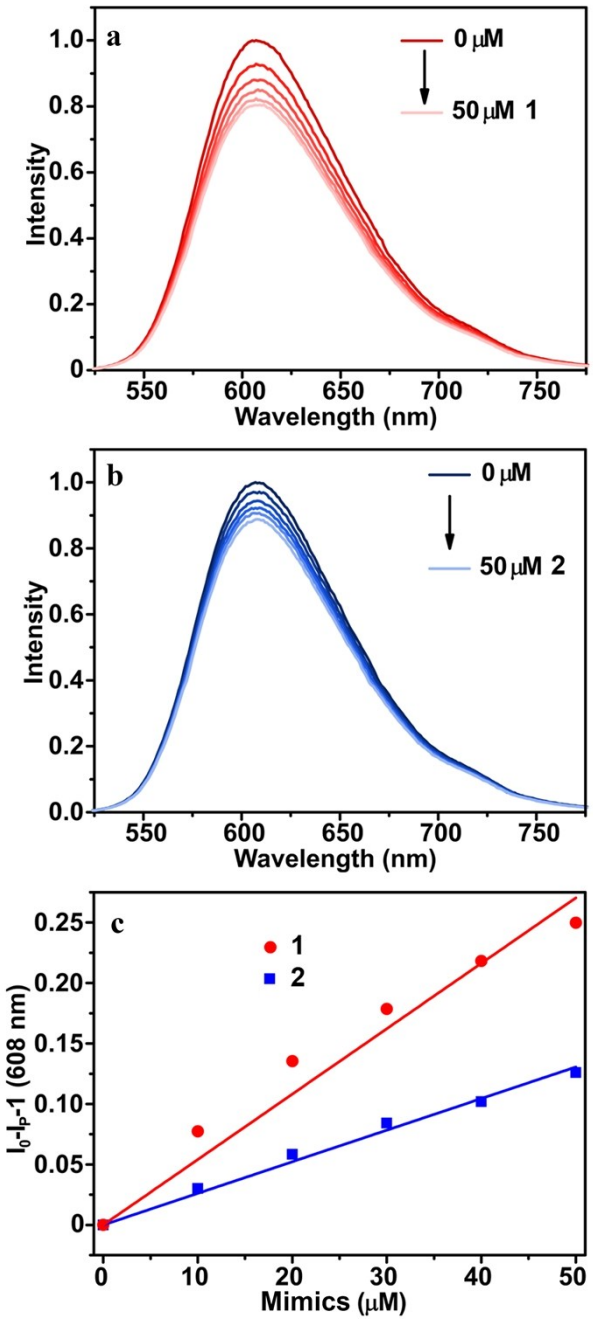

Fig. S8 Emission quenching of $Ru(bpy)_3Cl_2$ (0.10 mM) with progressive addition of **1** (**a**) and **2** (**b**); the corresponding Stern-Volmer plot of $[I_0/I_P - 1]$ *vs* the concentration of mimics (**c**).

10. Transient absorption and kinetics recovery of $Ru(bpy)_3Cl_2$ systems.

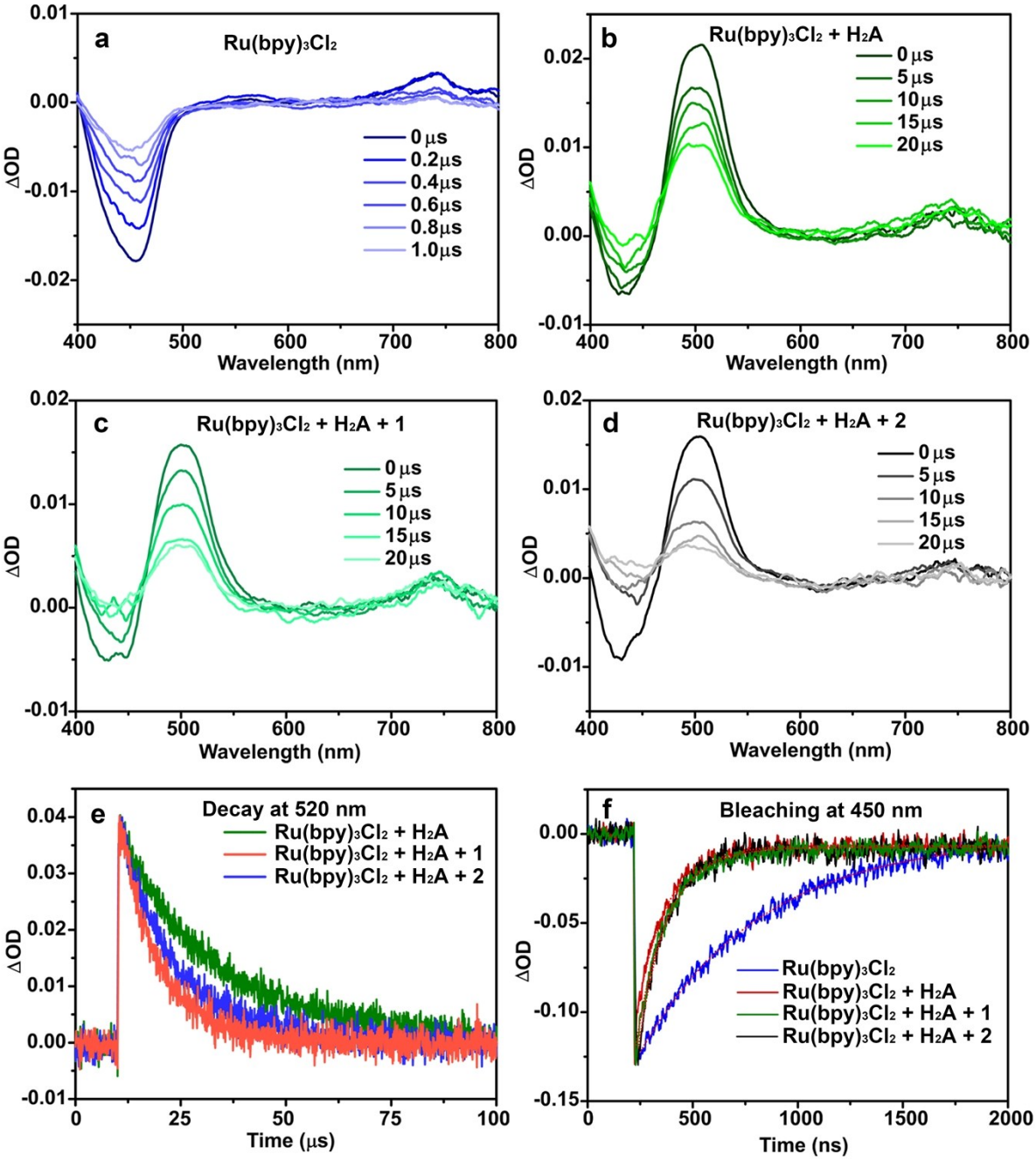

Fig. S9 The transient absorption of $Ru(bpy)_3Cl_2$ (0.10 mM) (**a**), $Ru(bpy)_3Cl_2$ + H_2A (0.20 M) (**b**), $Ru(bpy)_3Cl_2$ + H_2A + **1** (0.01 mM) (**c**) and $Ru(bpy)_3Cl_2$ + H_2A + **2** (0.01 mM) (**d**) in aqueous solution at pH 4.0; the corresponding recovery kinetics of transient decay recovery monitored at 520 nm (**e**) and transient blenching recovery monitored at 450 nm (**f**) for $Ru(bpy)_3Cl_2$ (0.10 mM), H_2A (0.20 M) and [FeFe]-H_2ase mimics (0.01 mM), upon laser excitation at 430 nm.

11. Emission quenching of CdSe QDs by 1 and 2.

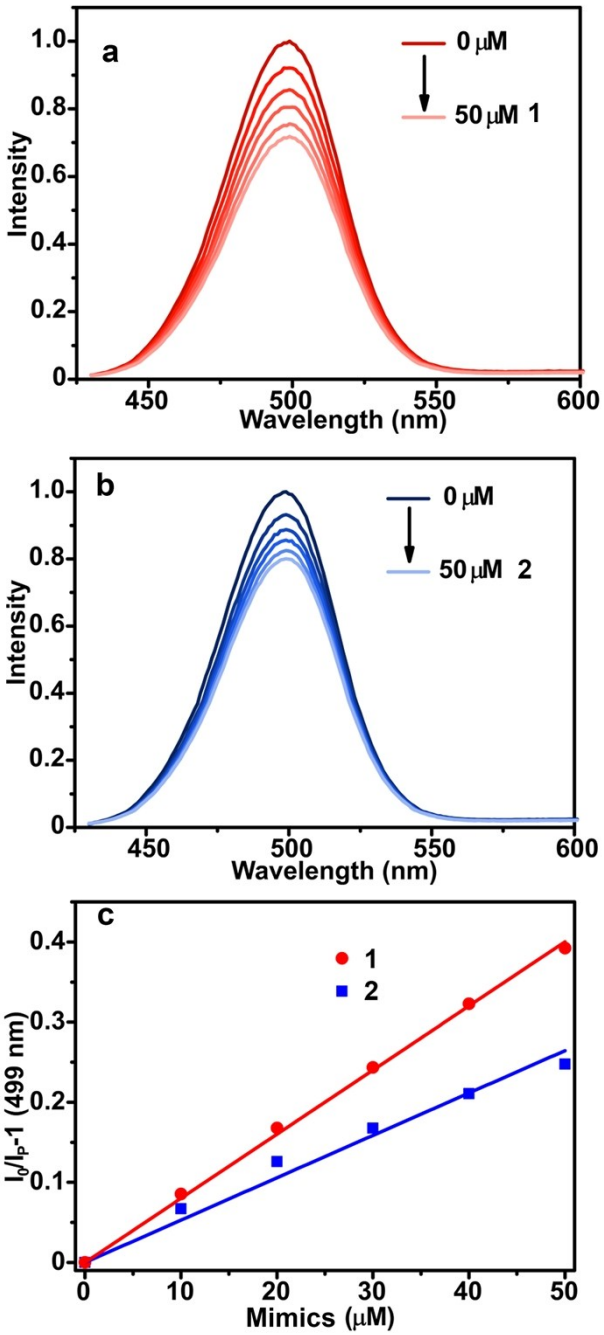

Fig. S10 Emission quenching of MPA-CdSe QDs (2.08 μM) with progressive addition of **1** (**a**) and **2** (**b**); the corresponding Stern-Volmer plot of [$I_0/I_P - 1$] *vs* the concentration of mimics (**c**).

12. Transient absorption of CdSe QDs.

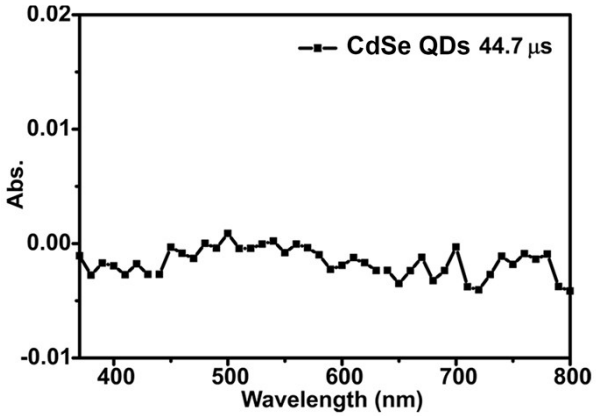

Fig. S11 Transient absorption spectra of CdSe QDs (2.08 μM) in aqueous solution at pH 4.0.

13. Spectroelectrochemical absorption spectra of [FeFe]-H_2ase mimics and TFA.

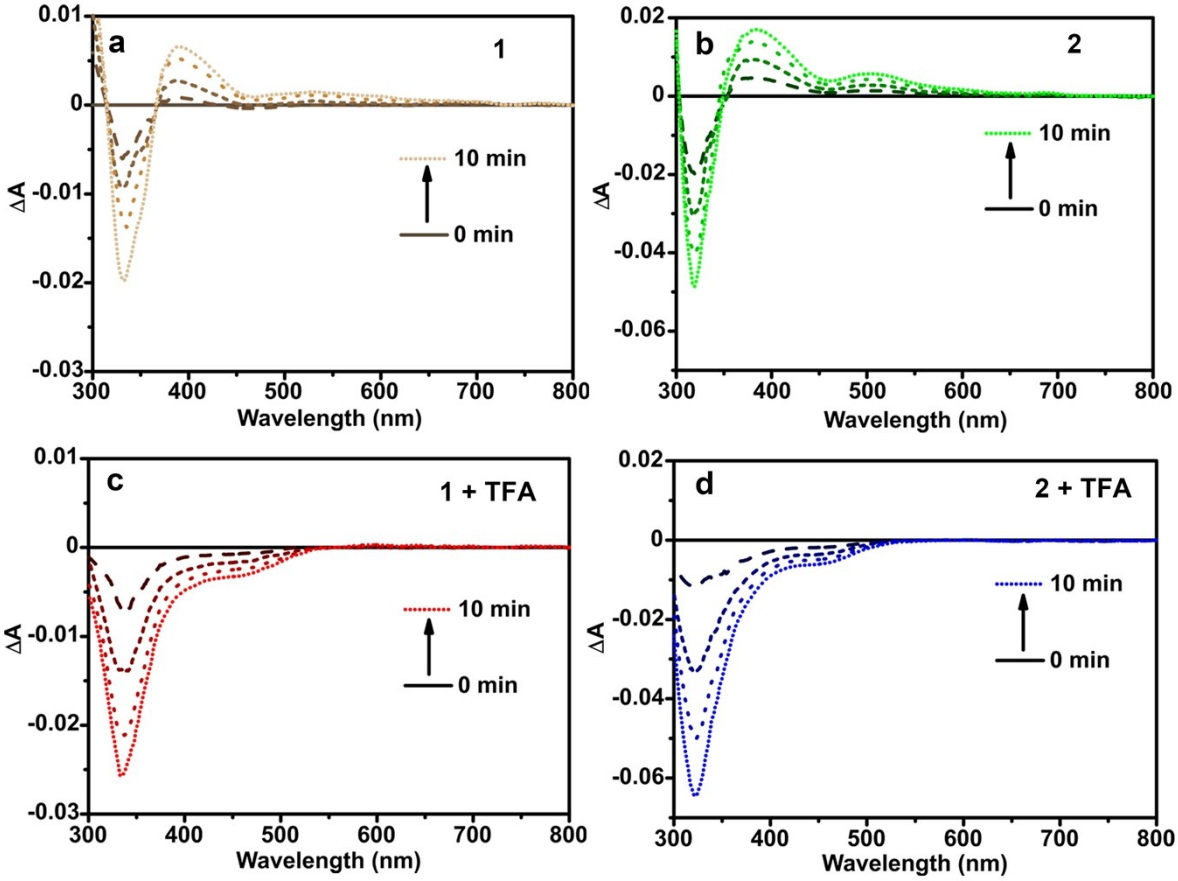

Fig. S12 Spectroelectrochemical absorption spectra of [$Fe^{I}Fe^{0}$] by reduction of [FeFe]-H_2ase mimics at -1.4 V relative to SCE (-1.16 V *vs* NHE): (**a**) **1** (0.1 mM); (**b**) **2** (0.1 mM); (**c**) **1** (0.1 mM) and TFA (1.0 mM); (**d**) **2** (0.1 mM) and TFA (1.0 mM).

14. Emission quenching of CdSe QDs by NaHA.

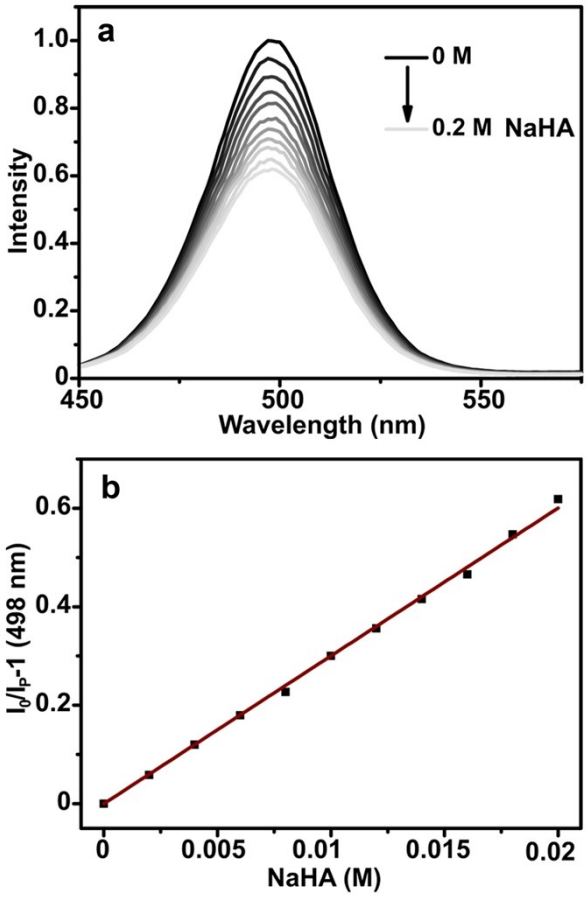

Fig. S13 The emission queching of MPA-CdSe QDs by NaHA (**a**); the corresponding Stern-Volmer plot of $[I_0/I_P - 1]$ of MPA-CdSe QDs *vs* the concentration of NaHA (**b**).